Supplementary Material

A Benchmark Simulator for Advanced Control of Ethanol Steam Reforming

Mateo Arcila-Osorio, Francesco Destro, Carlos Ocampo-Martinez, Jordi Llorca, Richard D. Braatz

1. Dependence of the model solution on the number of discretization points

To solve the set of partial differential equations (PDEs) arising from the ethanol steam reforming (ESR) and hydrogen separation process model, the method of lines (MOL) is applied. Thus, transforming the spatially distributed system into a set of ordinary differential equations (ODEs) through spatial discretization. This section presents a discussion about how the number of discretization points affects the accuracy, stability, and computational performance of the numerical solution.

The spatial derivatives of the states (concentrations and temperature) are approximated using a first-order finite difference upwind scheme, i.e.,

$$\frac{\partial x}{\partial z} \approx \frac{x(k) - x(k-1)}{\Delta z}, \tag{1}$$

where x is the corresponding state, z is the axial position variable, k is the discrete time step, and Δz is the distance between two spatial discretization points, which is determined as a function of the specify number of discretization points, namely n, for each stage in the staged-separation membrane reactor (SSMR). All simulations reported in this discussion were performed using MATLAB® R2023a on a laptop equipped with an AMD Ryzen 5 3500U processor with Radeon Vega Mobile Graphics (2.10 GHz) and a total memory of 8.0 GB RAM.

The simulation case selected to compare different values of n consist of running the model in open loop for 1 min in Mode 1 of normal operating conditions (see Table 2 in the paper). The simulation begins with initial conditions corresponding to steady-state axial profiles of species concentrations and temperature. After 0.4 min of simulation time,

a step change is introduced in the inlet ethanol molar flow rate (from 0.0021 to 0.0024 mol/min). Then, the dynamic response of the hydrogen concentration at the reforming stage outlet is observed. The result of this simulation case for $n \in \{50, 200, 400, 600\}$ is shown in Figure S1. All simulations exhibit the same overall behavior, characterized by a step-like increase in hydrogen concentration around 0.6 min. However, differences in the response become evident during the transient, as outlined below.

- The solution with $n = 50$ shows noticeable deviation from the other curves, with a smoother rise and slower convergence to the final steady-state value.
- Simulations with $n = 200$ and $n = 400$ show improved accuracy, with a sharper transient and faster settling. It is also noticed that the system presents an inverse response, initially decreasing the concentration before increasing it.
- The response with $n = 600$ shows only marginal improvement over $n = 400$, suggesting that further increasing the discretization points offers minimal additional benefit.

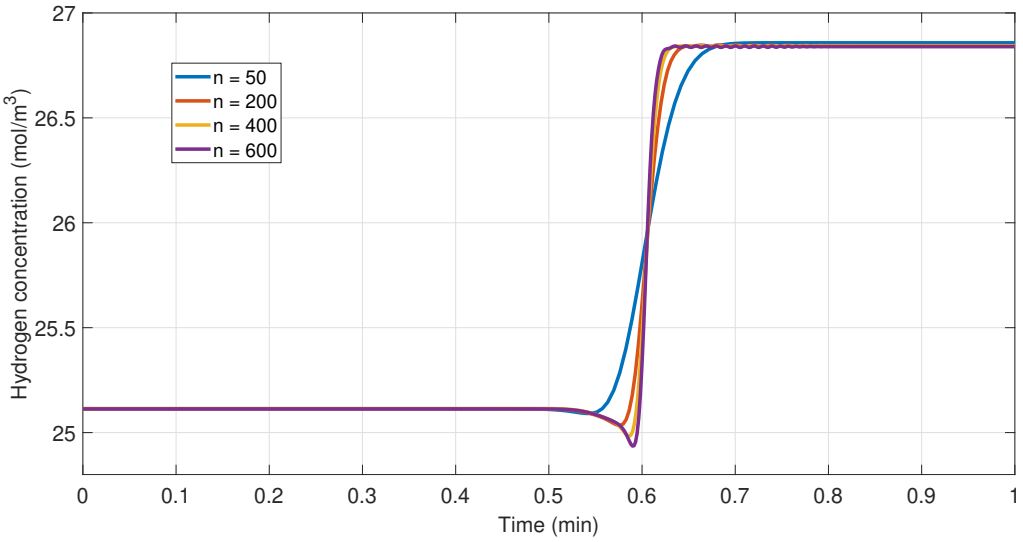

Figure S1. Outlet hydrogen concentration response to a step change (at $t = 0.4$ min) in the inlet ethanol molar flow rate (from 0.0021 to 0.0024 mol/min) for different numbers of discretization points.

The computational time required to run the simulations varies significantly with the number of discretization points. For $n = 50$, the simulation completes in approximately 2 s. As the discretization is refined, the computational time increases substantially. For $n = 200$, the simulation takes around 57 s, while for $n = 400$, the time required grows to 500 s. Certainly, the simulation with $n = 600$ is the most computationally demanding, requiring approximately 2100 s.

While increasing the number of spatial discretization points generally improves the resolution and accuracy of the simulation, it can also introduce numerical challenges.

In this study, simulations with more than 400 discretization points began to show signs of numerical instability, such as oscillations before setting the final steady state. These issues are likely due to increased stiffness in the resulting system of equations, which are common in MOL approaches when the spatial grid becomes excessively fine. Although the $n = 600$ case should potentially follow the expected physical trends, the signs of instability and significantly higher computational cost make it unsuitable as a reference solution. The simulation with $n = 400$ discretization points is selected as the reference case for comparing other simulations, as it presents much less oscillations and shows final steady-state convergence similar to $n = 600$.

For each simulation, the output hydrogen concentration over time is compared to the reference case ($n = 400$). Then, the relative error (%) is calculated as

$$e(t) = \frac{C_n(t) - C_{400}(t)}{C_{400}(t)} \times 100, \tag{2}$$

where $C_n(t)$ is the hydrogen concentration at time t for a given number of points n. The relative errors for the cases $n \in \{50, 200, 600\}$ are shown in Figure S2. Certainly, the relative errors increase during the transient response of the system, with the largest relative error occurring in the simulation with fewer discretization points. However, the simulations remain relatively close to each other.

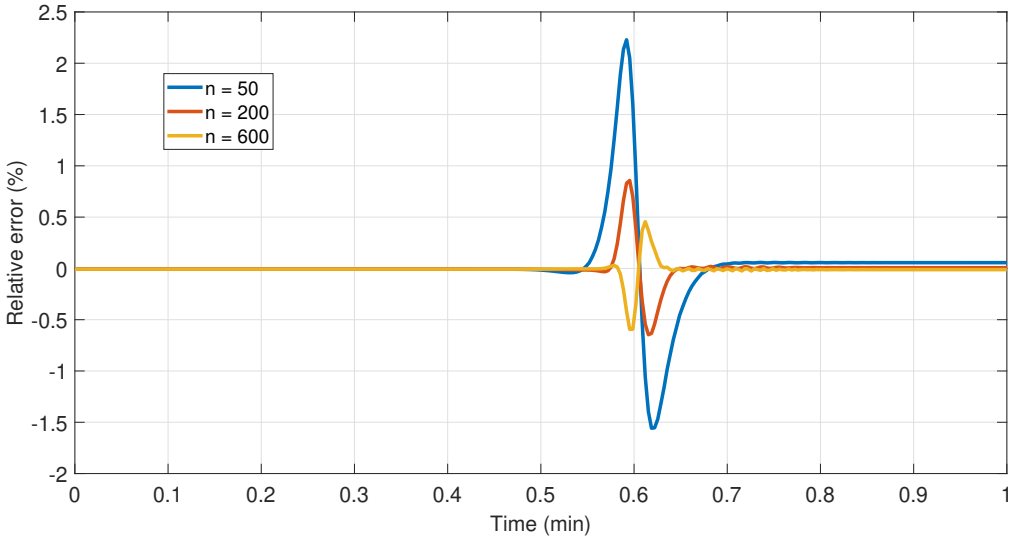

Figure S2. Relative errors of the simulations with $n \in \{50, 200, 600\}$ with respect to the simulation with $n = 400$.

Table S1 summarizes the maximum transient and steady-state relative errors, along with the computational times required for the simulations. Although the simulation with $n = 50$ exhibits the largest relative errors in both the transient and steady-state phases, the magnitude of these errors is negligible for practical purposes. Furthermore, this simulation is the only one that provides a reasonable computational time, making

it suitable for use in estimation and control tasks. For these reasons, the benchmark simulator model is formulated with a fixed value of $n = 50$.

Table S1. Maximum transient and steady-state relative errors of the simulations compared to $n = 400$, with the corresponding computational times.

n	Transient state (%)	Steady state (%)	Time (s)
50	2.20	0.056	2
200	0.85	0.007	57
400	-	-	500
600	0.59	0.012	2100

2. Initial conditions

The benchmark simulator proposes two different scenarios as starting points for the SSMR simulation.

2.1. Axial profiles of species concentration and temperature

In this scenario, both the reforming and separation stages begin from predefined steady-state axial profiles of species concentrations and temperature according to the specific mode of normal operating conditions, as can be seen in Figures S3, S4, and S5.

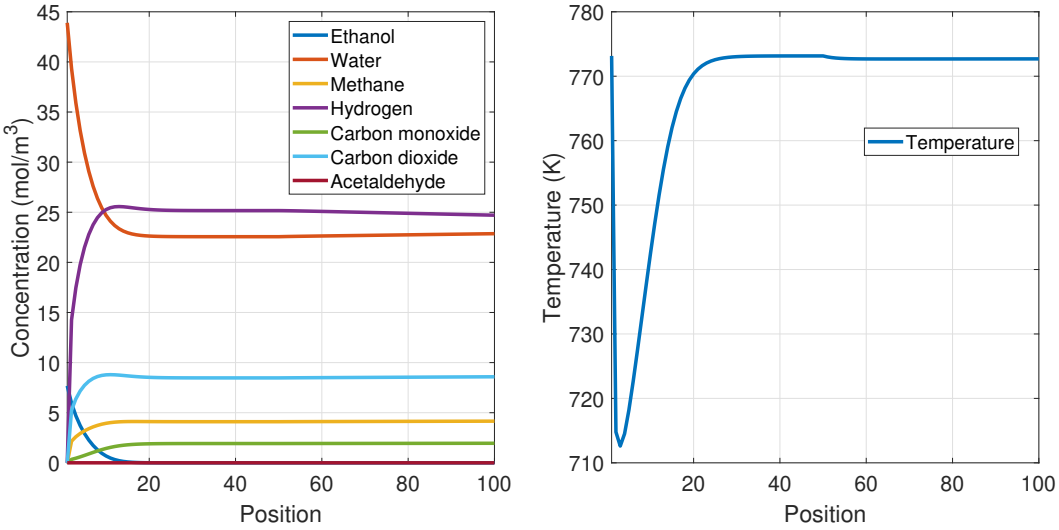

Figure S3. Axial profiles of species concentration and temperature for Mode 1 of normal operating conditions with $n = 50$.

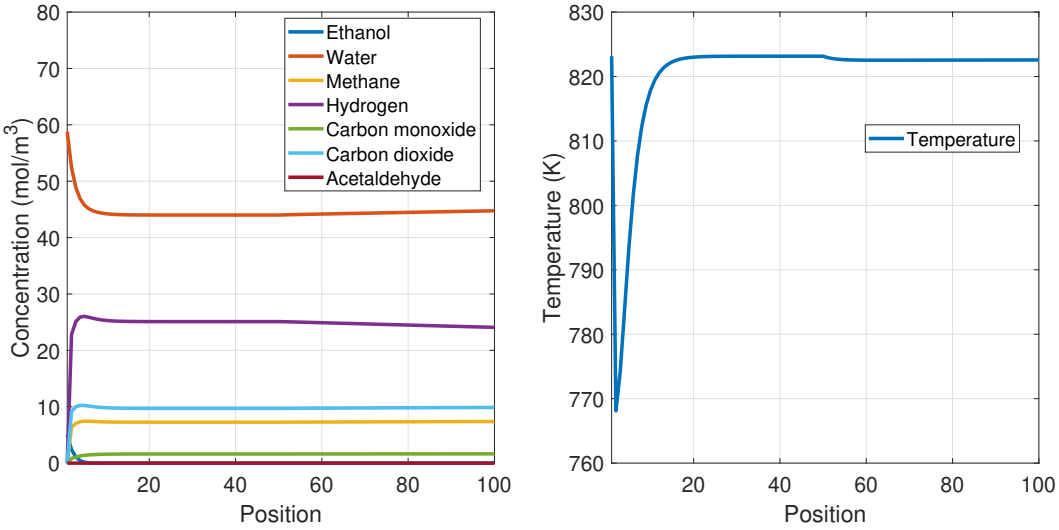

Figure S4. Axial profiles of species concentration and temperature for Mode 2 of normal operating conditions with $n = 50$.

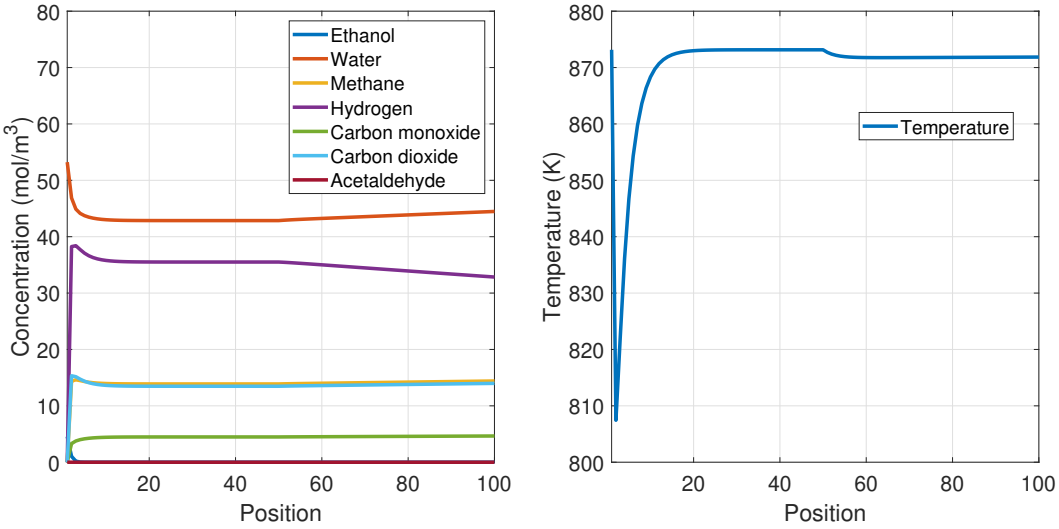

Figure S5. Axial profiles of species concentration and temperature for Mode 3 of normal operating conditions with $n = 50$.

2.2. Reactor filled with only steam with uniform temperature

In this scenario, the SSMR starts from a condition in which only steam, without ethanol, is flowing through the device, so neither chemical reactions nor membrane separation take place. The corresponding steam and temperature profiles for each normal operating mode are shown in Figures S6, S7, and S8.

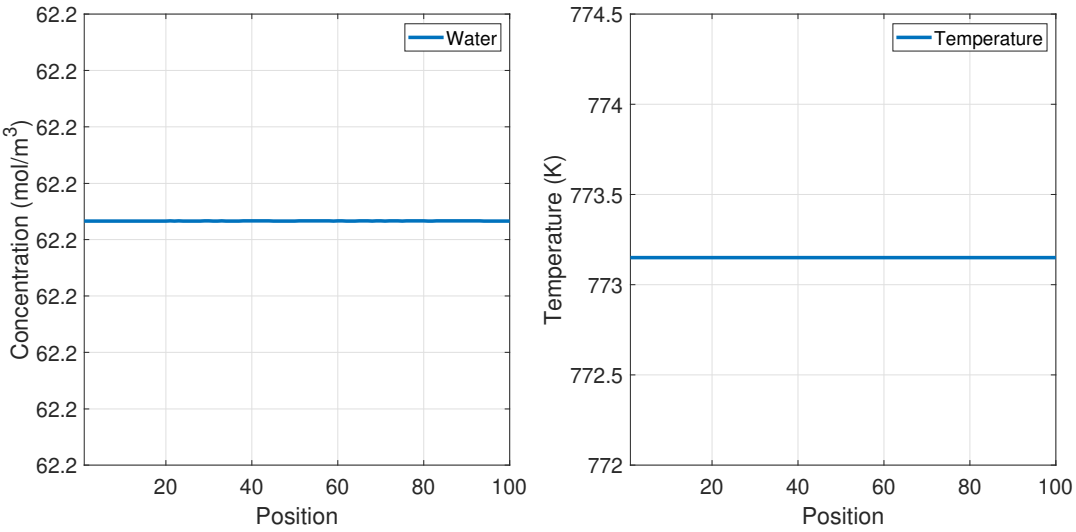

Figure S6. Starting value of water concentration and temperature for Mode 1 of normal operating conditions with $n = 50$.

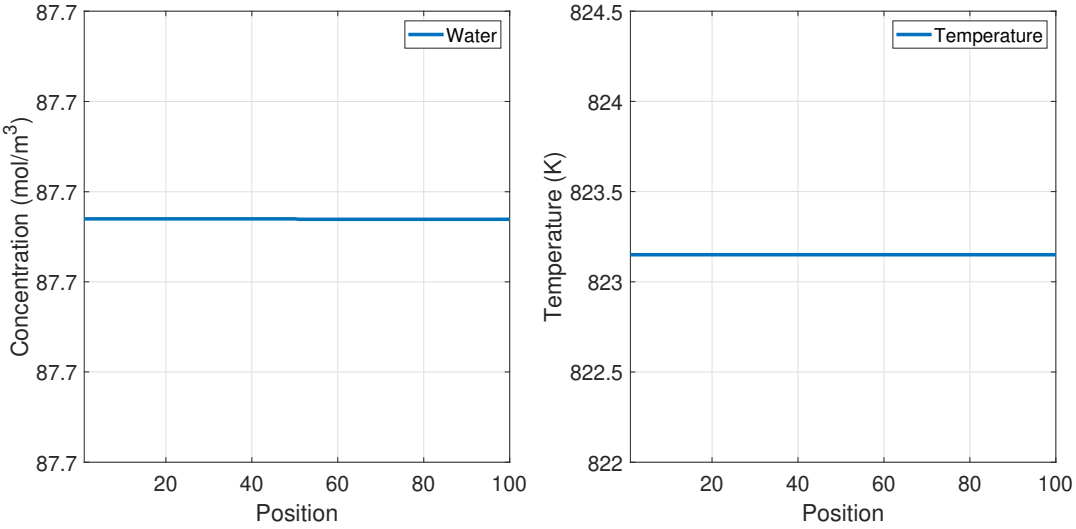

Figure S7. Starting value of water concentration and temperature for Mode 2 of normal operating conditions with $n = 50$.

3. PID controller performance in tracking a set-point profile for pure hydrogen production under Modes 2 and 3

The controller was operated with the same tuning parameters used in Case Study 1 for Mode 1. The results reveal a strong dependence of controller effectiveness on the operating mode. In Modes 2 and 3 (see Figures S9 and S10), the closed-loop dynamics exhibit

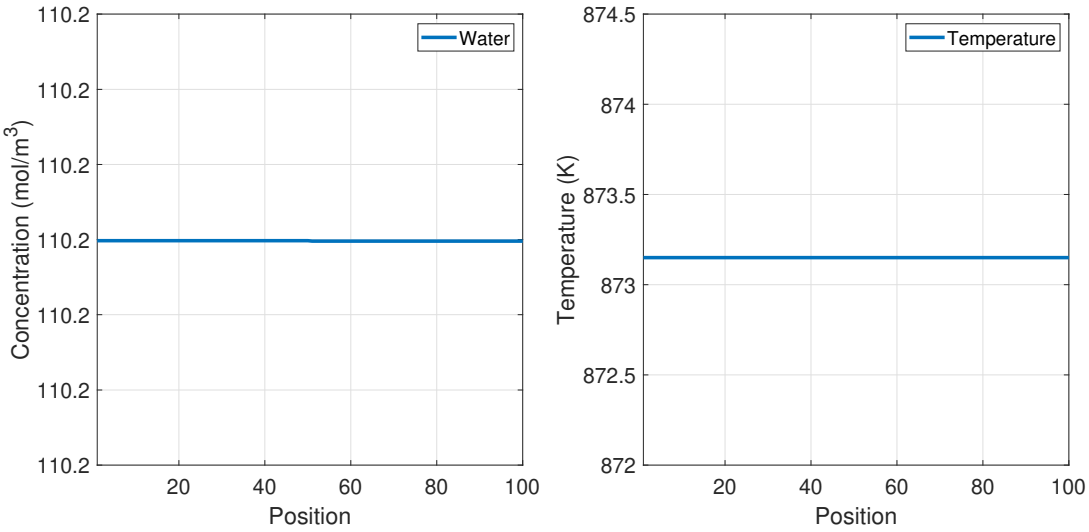

Figure S8. Starting value of water concentration and temperature for Mode 3 of normal operating conditions with $n = 50$.

pronounced oscillations and prolonged settling times. Moreover, in some regions of operation the system shows virtually no response to set-point changes, as the control action is limited by saturation of the sole manipulated variable, the inlet ethanol flow. These observations underscore the limitations of fixed-parameter PID control and motivate the use of gain-scheduled or adaptive strategies to preserve stability and performance across varying operating conditions. More importantly, they highlight the advantages of advanced control approaches, such as model predictive control (MPC), which can explicitly account for input and output constraints, adapt to changes in the operating regime, and optimize control performance in ways that conventional PID tuning can not achieve.

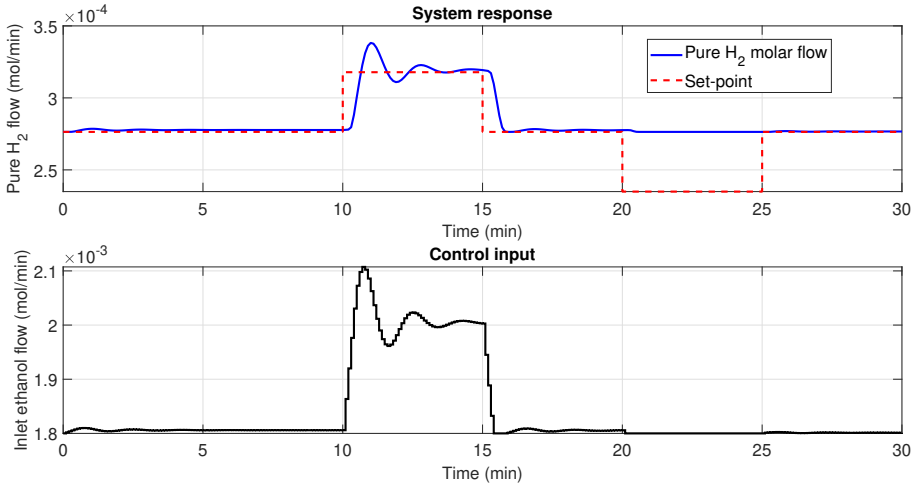

Figure S9. Tracking a set-point profile starting from Mode 2 of normal operating conditions. Top: pure hydrogen flow (blue) compared to the set-point trajectory (red dashed line). Bottom: inlet ethanol molar flow (control input).

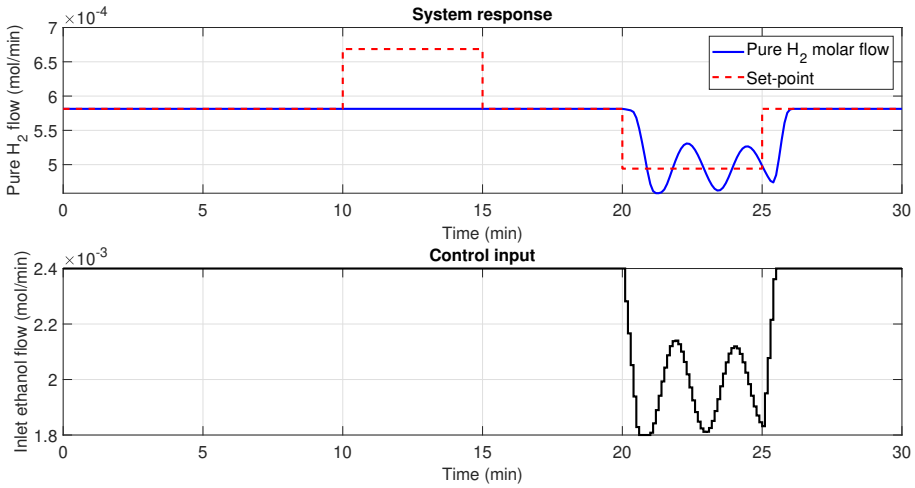

Figure S10. Tracking a set-point profile starting from Mode 3 of normal operating conditions. Top: pure hydrogen flow (blue) compared to the set-point trajectory (red dashed line). Bottom: inlet ethanol molar flow (control input).